Cell Cycle 12:19, 3203–3218; October 1, 2013; © 2013 Landes Bioscience

Measurement and modeling of transcriptional noise in the cell cycle regulatory network

David A Ball[1], Neil R Adames[1], Nadine Reischmann[1], Debashis Barik[2], Christopher T Franck[1,3], John J Tyson[1,2], and Jean Peccoud[1,4,*]

[1]Virginia Bioinformatics Institute; Virginia Tech; Blacksburg, VA USA; [2]Department of Biological Sciences; Virginia Tech; Blacksburg, VA USA; [3]Department of Statistics; Virginia Tech; Blacksburg, VA USA; [4]ICTAS Center for Systems Biology of Engineered Tissues; Virginia Tech; Blacksburg, VA USA

Keywords: cell cycle, stochastic modeling, gene expression noise, *Saccharomyces cerevisiae*, single mRNA FISH

Abbreviations: CDK, cyclin-dependent kinase; CKI, cyclin-dependent kinase inhibitor; FACS, fluorescence-activated cell sorting; FISH, fluorescence in situ hybridization; GFP, green fluorescent protein; ODE, ordinary differential equation; RENT, regulator of nucleolar silencing and telophase exit; SBF, SCB-binding factor; SSA, stochastic simulation algorithm; Q-Q plot, quantile-quantile plot

Fifty years of genetic and molecular experiments have revealed a wealth of molecular interactions involved in the control of cell division. In light of the complexity of this control system, mathematical modeling has proved useful in analyzing biochemical hypotheses that can be tested experimentally. Stochastic modeling has been especially useful in understanding the intrinsic variability of cell cycle events, but stochastic modeling has been hampered by a lack of reliable data on the absolute numbers of mRNA molecules per cell for cell cycle control genes. To fill this void, we used fluorescence in situ hybridization (FISH) to collect single molecule mRNA data for 16 cell cycle regulators in budding yeast, *Saccharomyces cerevisiae*. From statistical distributions of single-cell mRNA counts, we are able to extract the periodicity, timing, and magnitude of transcript abundance during the cell cycle. We used these parameters to improve a stochastic model of the cell cycle to better reflect the variability of molecular and phenotypic data on cell cycle progression in budding yeast.

Introduction

The eukaryotic cell division cycle is a complex process in which cells grow, replicate their DNA, and then partition their replicated chromosomes and organelles between 2 new daughter cells. These events are coordinated by a family of cyclin-dependent protein kinases (CDKs), whose activities are controlled by a complex network of interacting proteins. The budding yeast cell cycle is regulated by a single, constitutively expressed CDK (Cdc28), whose activity and substrate specificity change in a consistent manner during each stage of the cell division cycle.[1-5] The activity of Cdc28 in budding yeast is regulated by periodic changes in the availability of protein cofactors, called cyclins, each of which is produced and degraded during a specific phase of the cell cycle. Kinases, phosphatases, and CDK-inhibitory proteins (CKIs) modify the activities of these cyclin–CDK complexes. The abundances of the cyclins and many other regulatory proteins change during progression through the cell cycle because cyclin–CDK activity regulates their periodic synthesis and degradation.

Like any gene or protein regulatory network, the cell cycle is a noisy process; in genetically identical populations, there is significant cell-to-cell variation even in a uniform environment.[6] The sources of non-genetic variation in gene expression are a combination of intrinsic noise (the probabilistic nature of transcription and translation events resulting from the low abundance of transcription factors, their target genes, and transcripts) and extrinsic noise (such as inequalities in the partitioning of cellular components during division).[7] The abundance of a transcript or protein in a cell at any given time depends on the relative rates of synthesis and degradation and can be adequately described as a stochastic birth–death process with exponentially distributed waiting times.[6]

Mathematical modeling is now an integral component of cell cycle research. Computational biologists have developed models that are consistent with diverse sets of experimental data.[8-17] Models have helped predict previously unknown interactions that could be tested experimentally.[8,13,14,18-24] The first generation of models were "deterministic", relying on nonlinear ordinary differential equations (ODEs) to capture the viability (and other phenotypic characteristics) of dozens of mutants of the cell cycle control system.[25] However, other aspects of cell cycle progression, such as variability in interdivision time or cell size at division, cannot be explained by deterministic models.[12] To

*Correspondence to: Jean Peccoud; Email: peccoud@vt.edu
Submitted: 04/25/2013; Revised: 08/22/2013; Accepted: 08/23/2013
http://dx.doi.org/10.4161/cc.26257

account for these characteristics, along with the partial viability of some mutants, requires "stochastic" models of cell cycle progression.[8,14]

The first stochastic models of the cell cycle were derived from deterministic models by introducing extrinsic noise associated with partitioning of cellular components during cell division,[26] by introducing Gaussian white noise into reaction rate equations,[27] or by modifying Boolean deterministic models.[28-32] However, experiments in yeast cells with increasing gene dosage suggest that most noise in the cell cycle is a consequence of small copy number per cell of some molecular regulators, especially in G_1 phase of the cell cycle.[14] The early phenomenological models of noise in the cell cycle are not adequate to analyze the role of intrinsic noise in cell cycle fluctuations, which requires explicitly modeling molecular interactions at their source. Initially, stochastic models focused on protein activity levels and protein–protein interactions, since they are the products of gene expression and the agents of cellular activity.[26,27,29,31,32] By combining time-lapse microscopy, microfluidics, and image processing, it has been possible to observe in single cells the trajectories through the cell cycle of regulator proteins tagged with fluorescent protein domains.[14,23,33,34] However, cell cycle control also involves a complex system of transcriptional regulation. In fact, very little gene expression noise can be explained solely in terms of protein synthesis and degradation. A dominant proportion of intrinsic noise is the low abundance of mRNA.[11] Therefore, to develop better predictive stochastic models of cell cycle regulation, one must account quantitatively for the fluctuations of mRNA abundances in individual cells.

Accurate simulation of mRNA abundances, which are likely to be on the order of 5–10 molecules per yeast cell, requires the use of the Gillespie stochastic simulation algorithm (SSA), which is based on the assumption that the fluctuating reactions are pseudo-elementary, i.e., that they are adequately described by mass-action kinetics.[35] Because most deterministic models of cell cycle regulation rely heavily on complex rate laws (Michaelis–Menten kinetics, Hill functions, zero-order ultrasensitivity), they are not easily converted into mass-action-type models, suitable for simulation by Gillespie SSA.[36] To investigate the roles of intrinsic and extrinsic noise in cell cycle variability, Kar et al.[11] performed this conversion on a simple deterministic model of the budding yeast cell cycle. Using Gillespie SSA, they showed that intrinsic noise dominates over extrinsic noise in determining the variability of cell size and cell cycle timing in budding yeast. However, to obtain the correct level of noise, they had to use mRNA abundances 4 times greater than the values reported on the basis of microarray studies.[11] Also, they had to use mRNA half-lives (0.2–5 min) considerably shorter than the values reported on the basis of microarray studies.[11]

A year later, Barik et al.[10] presented a more realistic model of budding yeast growth and division, based on the idea that multisite phosphorylation of key cell cycle regulators is the primary source of nonlinearity in the control system. Even though the overall effect of multiple phosphorylations on protein behavior is nonlinear (i.e., switch-like), each phosphorylation event can be described by a mass-action rate law. Hence, the model can be simulated deterministically, by solving the nonlinear ODEs, or stochastically, by applying Gillespie SSA. The deterministic version of the model accurately reflected G_1/S size control and timing. The stochastic version accurately reproduced variability in cell cycle progression, provided that mRNA half-lives (1–5 min) are shorter than expected,[37] and mRNA levels (5–10 molecules per cell) are larger than expected.[38] The mRNA abundances in Barik's model[10] are in line with the values reported by Zenklusen and Singer[39] for non-cell cycle-related genes, based on FISH measurements. Because FISH data on cell cycle-related genes was lacking, it was impossible for Barik et al.[10] to calibrate their model accurately to the expected number and variability of regulatory mRNA molecules per cell.

In pursuit of more comprehensive and explanatory stochastic models of the cell cycle, we have used single mRNA FISH to measure the statistical distributions of transcripts for 16 cell cycle regulators in budding yeast.[39] We found that cell cycle regulators known to be constitutively expressed showed transcript abundance patterns consistent with a Poisson distribution. mRNA distributions of periodically expressed genes were best modeled as two-component Poisson distributions, reflecting their regulated high and low states of transcription.[40] We were also able to deduce the length of time in the cell cycle during which gene expression is elevated and the amplitude of the oscillations in gene expression.

We then used this data to refine the multisite phosphorylation model of Barik et al.[10] To match our observed distributions, we modified the model to allow complete dissociation of Whi5 from SBF and of Net1 from Cdc14, and we adjusted transcription and translation rates to produce *NET1* and *WHI5* mRNA distributions that better matched our observations. Because the only periodically expressed transcript in this model refers to the G_1/S cyclins (Cln1, Cln2, Clb5, and Clb6, called "ClbS" in the model), we were able to reproduce the two-component Poisson distributions of *CLN1* and *CLN2* mRNAs in our data set, but not of other periodic transcripts.

Results

Statistical distributions of mRNA abundance

Individual transcripts from 16 cell cycle genes were counted in single cells using single molecule FISH.[39] To this end, we used commercially available strains of *Saccharomyces cerevisiae* for which a GFP-coding sequence was inserted as an in-frame C-terminal fusion to a cell cycle control gene. A mixture of 5 fluorescently labeled oligonucleotides, each containing 5 internal fluorescent dye molecules, was hybridized to the GFP portion of these fused transcripts (**Fig. 1A**). Spots were visualized and counted with a spot-detection algorithm (**Fig. 1B and C**).[41] Cells lacking any GFP fusion elements were used as a negative control and showed virtually no fluorescent spots (**Table 1**), indicating a high specificity of the probes to the GFP transcripts. As a positive control, *MDN1* transcripts were counted using probes against the coding region of *MDN1* in a *MDN1–GFP* strain, and again using the same GFP probe set used for the other strains. Data from these 2 probe sets exhibited similar mRNA distributions,

and *MDN1* mRNA abundances were consistent with previous reports (**Table 1**).[42]

We then performed single mRNA FISH on asynchronous cultures of the 16 strains with GFP fused to a particular gene involved in cell cycle regulation. The average numbers of transcripts for each gene from one biological replicate are reported in **Table 1**. Similar results were obtained in 2 other biological replicates (**Table S1**). Our results, as well as those from other single mRNA FISH studies,[42,43] consistently showed mRNA levels roughly 4-fold higher than large-scale transcriptome studies (**Table S2**). This discrepancy is probably due to the method of normalization used in transcriptome studies to infer average transcript abundance per cell (for discussion of this issue, see **Supplementary Material**). In fact, all transcriptome studies are in good agreement with our mRNA FISH data when they are normalized to 60 000 transcripts/cell (**Table S2**).

Test of transcriptional regulation

The genes studied here are involved in the M/G_1 and G_1/S transitions. Half of them are known to be constitutively expressed, and the other half are transcriptionally regulated (**Table 1**; **Fig. S1**). Furthermore, the periodic genes represent most of the known expression mechanisms for cell cycle genes, with the expression of at least one gene peaking at every stage of the cell cycle (**Fig. S1**).

We used maximum likelihood estimation to fit the mRNA data to a Poisson distribution. We found that *BCK2*, *BUB2*, *CDC15*, *LTE1*, *MAD2*, *MCM1*, and *NET1* mRNAs all fit well to this distribution, confirming that these genes are constitutively transcribed (**Fig. 1D; Table 1; Table S1; Fig. S2**).[44-48]

Transcript data for 6 of the genes (*CDC6*, *CDC20*, *CLB2*, *CLN1*, *CLN2*, and *SIC1*) did not fit a Poisson distribution (**Table 1; Table S1**). Each of these distributions has a clearly visible shoulder or tail in the histogram (**Fig. 1D**; **Fig. S2**), consistent

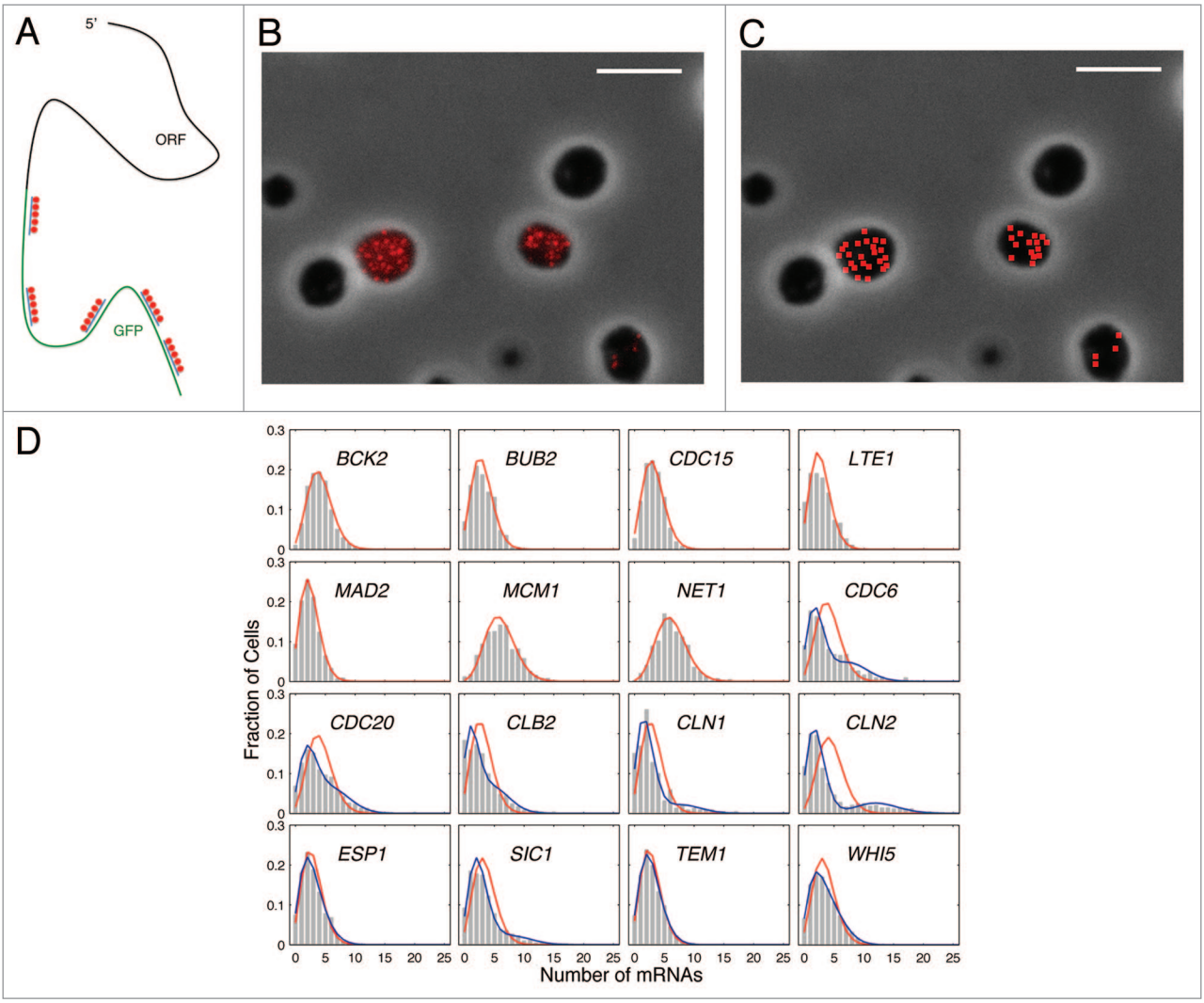

Figure 1. Summary of single mRNA FISH method and mRNA distributions. (**A**) Schematic of how the FISH probes hybridize to target mRNAs. (**B**) Example image showing individual mRNA molecules. Image is a maximum intensity projection of a z-series with merged phase-contrast and fluorescence channels. (**C**) Detected single transcripts. The image in the left panel was processed as described in "Materials and Methods" to detect spots of single mRNAs. Scale bar = 5 μm. (**D**) Experimental distributions of mRNA for 16 cell cycle genes. Gray bars show the experimental histograms; red lines are the fit to a single component Poisson, and blue lines are the fit to a two-component Poisson. Data are from the biological replicate shown in **Table 1**. Similar results were obtained in 2 other biological replicates (**Table S1**).

with the hypothesis that these genes switch between 2 states of high and low transcription. Not surprisingly, all of these genes are annotated as periodically expressed (**Table 1**). We found that the distributions of mRNA abundance of these 6 genes are described well by two-component Poisson distributions, confirming that they have 2 expression states in the population (**Fig. 1; Table 1; Table S1; Fig. S2**).

Similar results were obtained in 3 biological replicates (**Table 1; Table S1**). There was generally good agreement between previous gene annotations and the outcomes of statistical tests to

Table 1. Cell cycle mRNA distributions in asynchronous populations and derived gene expression parameters

Gene	Periodic[a]	FISH mean ± 95% CI[b]	Single Poisson[c]		Two-component Poisson[d]				
			G test *P* value	ϕ^2 effect size	β ± 95% CI	λ_1 ± 95% CI	λ_2 ± 95% CI	G test *P* value	ϕ^2 effect size
BY4733 (WT no GFP)	No	0.08 ± 0.02							
MDN1 (MDN1 probes)	No	9.37 ± 0.23	0.02	0.04					
MDN1 (GFP probes)	No	9.20 ± 0.27	4.47E-05	0.01					
BCK2	No	4.16 ± 0.21	0.78	0.01					
BUB2	No	3.04 ± 0.13	9.87E-04	0.04					
CDC15	No	3.24 ± 0.13	0.18	0.01					
LTE1	No	2.73 ± 0.09	0.00	0.10					
MAD2	No	2.50 ± 0.10	0.69	4.22E-03					
MCM1	No	6.06 ± 0.22	4.10E-03	0.05					
NET1	No	6.20 ± 0.25	0.60	0.02					
CDC6	Yes	4.07 ± 0.20	0.00	0.99	0.67 ± 0.07	2.12 ± 0.26	8.08 ± 0.72	0.03	0.05
CDC20	Yes	4.16 ± 0.15	0.00	0.64	0.63 ± 0.08	2.47 ± 0.29	7.08 ± 0.61	0.09	0.02
CLB2	Yes	3.01 ± 0.10	0.00	0.74	0.65 ± 0.07	1.55 ± 0.20	5.69 ± 0.49	1.20E-10	0.07
CLN1	Yes	3.03 ± 0.23	9.99E-16	0.47	0.85 ± 0.07	2.03 ± 0.28	8.56 ± 1.53	2.02E-03	0.09
CLN2	Yes	4.45 ± 0.13	0.00	4.49	0.77 ± 0.03	2.09 ± 0.12	12.4 ± 0.55	5.92E-06	0.06
ESP1	Yes	2.89 ± 0.11	7.23E-07	0.05	0.62 ± 0.26	2.15 ± 0.42	4.09 ± 0.75	0.11	0.01
SIC1	Yes	3.44 ± 0.12	0.00	0.62	0.84 ± 0.03	2.47 ± 0.15	8.68 ± 0.79	4.46E-03	0.03
TEM1	Yes	2.83 ± 0.12	0.10	0.02	0.53 ± 0.68	2.17 ± 0.89	3.57 ± 1.09	0.75	3.19E-03
WHI5	Yes	3.45 ± 0.13	1.11E-16	0.15	0.52 ± 0.16	2.12 ± 0.41	4.90 ± 0.57	0.99	9.89E-04

[a]Expression of genes are ranked as cell cycle periodic by Cyclebase[46] and by ref. 59; [b]Transcripts/cell. The biological replicate from **Figure 1** is shown. Similar results were obtained in other replicates (**Table S1**); [c]Measured mRNA distribution fits to a Poisson distribution. G test of goodness of fit to a single Poisson distribution with λ = FISH Mean. ϕ^2 effect size. By convention, effect sizes of $\phi^2 \leq 0.09$ are considered small (green), $0.09 < \phi^2 < 0.25$ are considered medium (orange), and $\phi^2 \geq 0.25$ are considered large (red).[63] Null hypothesis for the *P* value is that the empirical data have a single Poisson distribution with mean λ; [d]Measured mRNA distribution fits to a two-component Poisson distribution. Same data set as for the single Poisson distribution. β, fraction of the population with low transcript levels. λ_1, mean transcripts/cell for the fraction of the population with low transcript levels. λ_2, mean transcripts/cell for the fraction of the population with high transcript levels. G test *P* values and ϕ^2 as for single-Poisson fit, but the null hypothesis is that the data have a two-component Poisson distribution with means λ_1 and λ_2.

differentiate constitutively expressed and transcriptionally regulated genes. In fact, there was an excellent correlation between whether a gene showed mRNA periodicity and whether the corresponding protein oscillates (**Table S3**).[33] In this context, it is notable that although *ESP1*, *TEM1*, and *WHI5* are ranked as periodic, their transcripts fit a single Poisson distribution in 2 of the 3 biological replicates, and neither Esp1-GFP nor Tem1-GFP display significant protein oscillations (**Table S3**).[33]

Timing and amplitude of mRNA oscillations

We next asked if the proportion of highly expressing cells in the asynchronous population correlated with the proportion of the cell cycle in which the gene is expressed. We compared our FISH experiments to mean expression profiles in Cyclebase, derived from 6 different microarray experiments using synchronized cells (**Fig. S1**). For each periodic gene, we compared the fraction of cells with high mRNA abundance (**Table 1**) to the fraction of the cell cycle time in which gene expression is ≥50% of the peak level (full-width half-maximum; **Fig. 2A–C**). The good correlation between FISH and microarray data (**Fig. 2C**) indicates that the proportion of highly expressing cells does indeed correspond to the proportion of cell cycle time during which the gene is expressed.

The two-component Poisson analyses produce mean transcript numbers for the highly expressing population (λ_2). It seemed reasonable to expect that the ratio between the mean transcript numbers for the highly expressing subpopulation and for the population as a whole would correlate with the peak expression level of the gene divided by its mean expression level in microarray experiments. In fact, comparison of the 2 data sets shows a strong correlation (**Fig. 2D**). Therefore, distribution analysis of single mRNA FISH yielded accurate values for the magnitude of change in gene expression for regulated genes.

The amplitudes of *CLB2* and *SIC1* expression did not match in FISH and microarray data (the amplitudes are much higher in Cyclebase). Consequently, these outliers were excluded from the correlation analysis reported in **Figure 2D**. Nevertheless, when these transcripts were included, the correlation of expression between FISH and microarray data was still good (R^2 = 0.38,

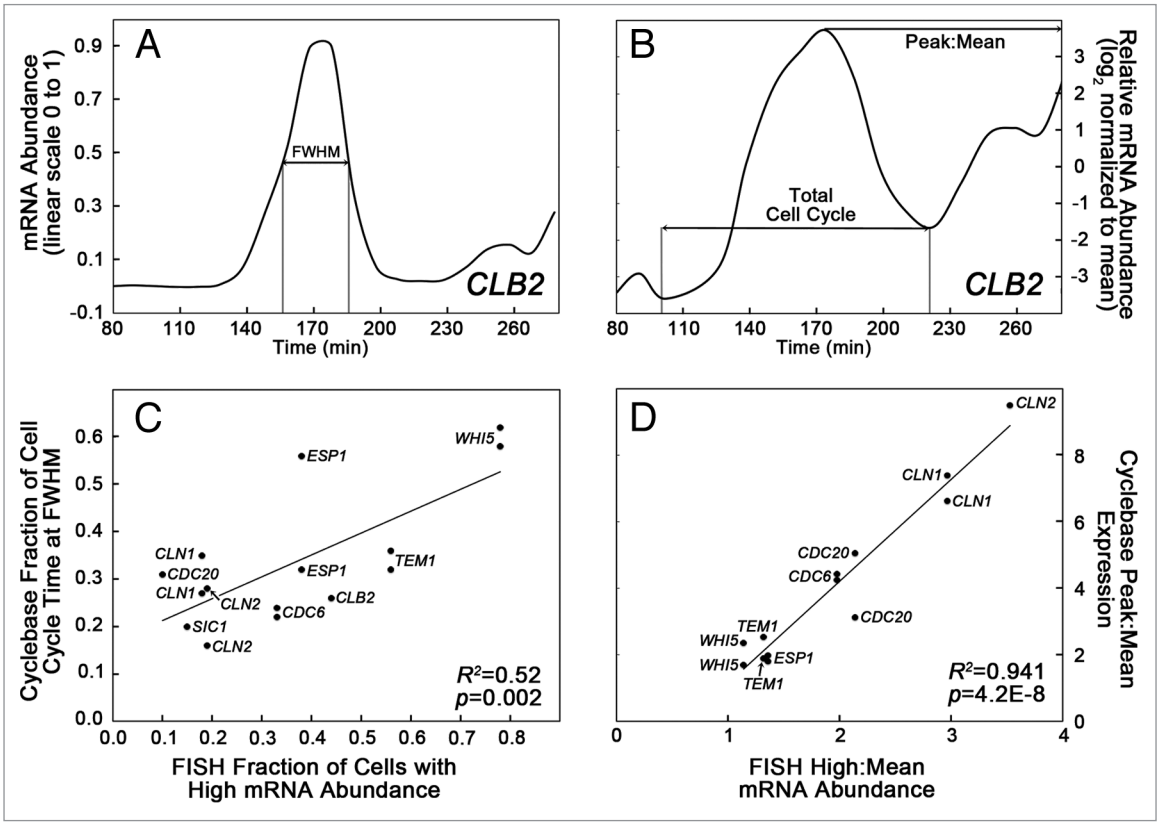

Figure 2. Correlation between the timing and magnitude of gene expression from FISH experiments and Cyclebase microarray experiments. (**A**) *CLB2* microarray data plotted on a linear scale with the minimum value set at 0 and the maximum set at 1. Used as an example of how we measure the length of time that the transcript level is greater than the half-maximum level (FWHM, full-width at half maximum). (**B**) *CLB2* microarray data on a $\log_2$ scale. Values are relative to the time-course mean. Used as an example of how we measure the peak:mean value and the total cell cycle time. (**C**) Correlation plot for each cell cycle gene showing fraction of the high expression population from FISH experiments (1 - β) compared with the fraction of cell cycle time in which transcript levels exceed FWHM level from Cyclebase. (**D**) Correlation plot for each periodic cell cycle gene showing the ratio of the mean transcript values of the high abundance population (λ_2) to the mean for the population from FISH experiments compared with the peak:mean values from Cyclebase. Data are from the biological replicate shown in **Table 1**. Similar results are obtained with all biological replicates. Values for *CLB2* and *SIC1* are not included (see text). Some genes have two peaks of expression in the Cyclebase data, producing two data points. R^2 values and *P* values from ANOVA statistical analysis of the linear regressions are shown. Null hypothesis for the *P* value is that there is no correlation between the FISH and Cyclebase data.

P = 0.018). The mismatch for *CLB2* and *SIC1* may be attributable to the methods used to synchronize cells and to register the data in Cyclebase. In the microarray experiments, the abundance of *CLB2* and *SIC1* transcripts is suppressed in the first portion of the expression plots (**Fig. S1**). For *CLB2*, expression levels are much lower at the beginning of the time-trace than the minimum attained in the subsequent cell cycle, despite the fact that *CLB2* levels should be high but decreasing in M phase. Similarly, *SIC1* levels are artificially low at the start (the initial M phase), but this is clearly an artifact of how Cyclebase registers the experiments using α factor or a temperature-sensitive *cdc28* allele (both of which arrest cells in G_1). By contrast, experiments using a temperature-sensitive *cdc15* allele, which arrests the cells in late M, did show an initial peak (**Fig. S1**). The lack of a starting peak for G_1-arrested cells is likely due to the fact that the "initial M phase" of the time-registered experiments actually occurs at the end of the second cell cycle, by which time synchrony is reduced. The underestimated expression levels for the first part of the time-course data for *CLB2* and *SIC1* result in lower overall means and inflated relative peak values for these genes. The synchronization method is not a problem for the other periodic genes, as they are expressed earlier in the cell cycle than *CLB2* and *SIC1*, before synchrony degenerates, and show 2 clear peaks in mRNA abundance, which produce more accurate overall means (**Fig. S1**). So, it appears possible that Cyclebase overestimates the magnitude of expression (peak:mean ratio) for *CLB2* and *SIC1*.

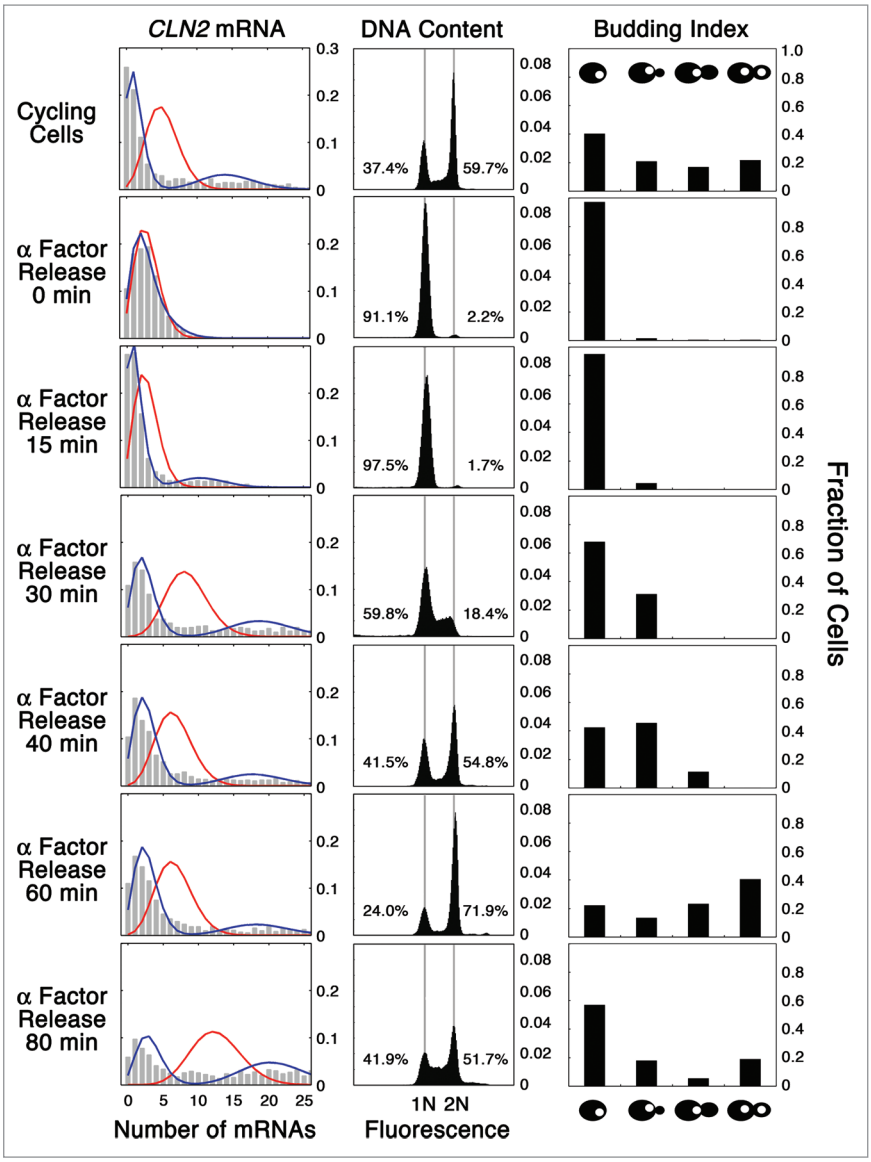

Figure 3. *CLN2* mRNA distribution changes during cell cycle progression. Single mRNA FISH was performed on α-factor synchronized *CLN2-GFP* cells. These cells were chosen, because *CLN2* expression is induced at the START transition and should be low in α-factor arrested cells (G_1). Cells were released from arrest (0 min) and allowed to proceed through the cell cycle. Samples were removed from the culture at the indicated times and processed for FISH, FACS analysis of DNA content, and to determine bud morphology as benchmarks for cell cycle progression. Left panel: *CLN2* mRNA cellular abundance distributions as determined by FISH. Also shown are single Poisson distributions (red line) and two-component Poisson distributions (blue line) fitted to the mean mRNA abundances. The Poisson parameters and statistics are provided in **Table 2**. Middle panel: DNA content as determined by FACS analysis with the proportions of 1N and 2N cells indicated as percentages. Percentages are not 100% because of incompletely stained cells that are not within the peaks. Right panel: the proportion of unbudded (G_1) cells, small-budded (<1/3 size of mother; S-phase) cells, large-budded cells with one nucleus (G_2/M), and large-budded cells with an elongated nucleus in the neck or in which both mother and bud contain a nucleus (anaphase/telophase).

Another possible explanation of the discrepancy is that our FISH data underestimated these oscillations due to saturation of the spot detection algorithm. We do not think this was the case, because 3 genes (*CLN1*, *CLN2*, *CDC20*) had higher absolute numbers of transcripts per cell than *CLB2* and *SIC1*, and these genes correlated well with the Cyclebase data (**Table 1; Fig. 2D**).

To demonstrate that the low and high expressing populations in the FISH results correspond to cell cycle periodicity of expression, we performed a time course experiment using synchronized *CLN2-GFP* cells and monitored *CLN2* mRNA levels relative to cell cycle progression, as determined by bud morphology and DNA content. As expected, *CLN2* mRNA abundance was low in cells arrested in G_1 by treatment with α-factor, and the single-cell mRNA levels fit a single-component Poisson distribution reasonably well (**Fig. 3; Table 2**). Within 30 min after release from G_1 arrest, the proportion of cells expressing high levels of *CLN2* mRNA increases, the mean transcript abundance of the high expressing population increases, and the mRNA abundances now fit two-component Poisson distributions (**Fig. 3; Table 2**). The shift in the cell population to higher *CLN2* mRNA abundance corresponded to S-phase entry as shown

by a corresponding shift of DNA content from 1N to 2N and by the appearance of small-budded cells (**Fig. 3**). A small population of high expressing cells persisted at later times, probably due to imperfect synchronization, since there were G_1- and S-phase cells throughout the experimental time course (**Fig. 3**).

A second peak in *CLN2* expression occurred at the 80 min time point as the cells entered a second cell cycle (**Fig. 3; Table 2**). In fact, *CLN2* expression appeared to be more robust in the subsequent cycle despite a clear degradation in synchrony compared with the 30 min time point, suggesting that α-factor treatment might initially suppress the accumulation of *CLN2* mRNA after cells are released.

Surprisingly, the proportion of cells that have no *CLN2* mRNA was a minor portion of the population throughout the time course, and the mean *CLN2* mRNA levels of the low expressing population remained relatively constant (**Fig. 3; Table 2**). The persistence of low expressing cells might be due to imperfect synchronization of the population, since there was a significant population of G_1–S cells even 60 min after release (**Fig. 3**). However, the proportion of low expressing cells was much higher than the fraction of G_1–S cells (e.g., 75% low expressing cells but only ~35% G_1-S cells at 60 min; **Fig. 3**), indicating that there is measurable *CLN2* basal transcription throughout the cell cycle.

Comparing mRNA and protein dynamics

Although we are examining only a small set of cell cycle-regulatory genes in this study, our results suggest that regulation of mRNA abundance is an excellent predictor for the regulation of protein abundance (**Table S3**). However, as revealed in multiple transcriptome-proteome studies, mRNA and protein steady-state levels are usually not well correlated (R^2 values are typically between 0.2–0.5).[49] To better understand the influence of mRNA dynamics on protein dynamics, we decided to test if there were any correlations between the amplitudes of mRNA and protein oscillations and between mRNA and protein abundances.

Unfortunately, we were unable to compare mRNA and protein abundances in the same cells, because GFP fluorescence is not well preserved using the single mRNA FISH protocol. However, we previously described protein dynamics for the same 16 GFP-tagged strains,[33] and we were able to compare the mRNA data from FISH to these protein data. We found that there was no significant correlation between the amplitudes of mRNA and protein oscillations (**Fig. 4A**, $P = 0.2$, null hypothesis is zero correlation). This poor correlation of mRNA to protein amplitudes probably reflects individual rate differences between synthesis and degradation of mRNA compared with protein. Furthermore, when we compared mean population levels of mRNA to protein (values are listed in **Table S3**), there was a mildly significant correlation reminiscent of transcriptome-proteome comparisons (**Fig. 4B**, black regression line, $P = 0.03$).[49] However, we found very strong correlations between mRNA and protein abundances when we grouped the data by constitutive or periodic mRNA (**Fig. 4B**, blue regression line $P = 1.8E\text{-}4$ and red regression line $P = 1.4E\text{-}3$, respectively). We were able to use the protein population means for these correlations, because all of the proteins exhibit normal or Poisson distributions and do not consist of widely distinct populations expressing low or high levels of protein as there is for mRNA (**Fig. S3**).

Although separating the genes by their regulation showed good mRNA:protein correlations, the slope of the linear regression for the periodic genes was much higher than that of the constitutive genes (**Fig. 4B**, red regression line m = 354.4 and blue regression line m = 57.2, respectively). There is no reason to suppose that translation efficiency is so exquisitely sensitive to mRNA concentration differences of a few molecules per cell, since translation rates are largely governed by initiation and elongation kinetics.[50,51] Instead, we postulated that the high slope of the correlation for periodic genes was due to the fact that most protein is produced in the high transcription state, and using

Table 2. Cell cycle-dependent *CLN2* mRNA distributions in synchronized cells and derived gene expression parameters

Cell cycle stage of CLN2 cells	FISH mean ± 95% CI[a]	Single Poisson[b]		Two-component Poisson[c]				
		G test *P* value	ϕ^2 effect size	β ± 95% CI	λ_1 ± 95% CI	λ_2 ± 95% CI	G test *P* value	ϕ^2 effect size
asynchronous from Table 1	4.45 ± 0.13	0.00	4.49	0.77 ± 0.03	2.09 ± 0.12	12.4 ± 0.55	5.92E-06	0.06
asynchronous	5.20 ± 0.11	0.00	18.08	0.70 ± 0.02	1.29 ± 0.08	14.46 ± 0.41	0 0.00	0.45
0 min α-factor release	2.94 ± 0.11	0.00	0.15	0.78 ± 0.14	2.25 ± 0.30	5.46 ± 1.09	0.03	0.02
15 min α-factor release	2.79 ± 0.11	0.00	2.78	0.83 ± 0.03	1.19 ± 0.09	10.86 ± 0.62	1.64E-07	0.08
30 min α-factor release	8.42 ± 0.19	0.00	23.77	0.64 ± 0.03	2.33 ± 0.15	19.10 ± 0.54	0.00	0.76
40 min α-factor release	6.61 ± 0.16	0.00	12.23	0.74 ± 0.03	2.54 ± 0.14	18.13 ± 0.66	0.00	0.57
60 min α-factor release	6.61 ± 0.19	0.00	11.51	0.75 ± 0.03	2.64 ± 0.16	18.66 ± 0.77	0.00	0.54
80 min α-factor release	12.59 ± 0.23	0.00	15.09	0.46 ± 0.03	3.14 ± 0.23	20.68 ± 0.47	0.00	0.92

[a]Transcripts/cell. Data are from cells shown in **Figure 3**; [b] Measured mRNA distribution fits to a Poisson distribution. G test of goodness of fit to a single Poisson distribution with λ = FISH Mean. ϕ^2 effect size. By convention, effect sizes of $\phi^2 \leq 0.09$ are considered small (green), $0.09 < \phi^2 < 0.25$ are considered medium (orange), and $\phi^2 \geq 0.25$ are considered large (red).[63] Null hypothesis for the *P* value is that the empirical data have a single Poisson distribution with mean λ; [c]Measured mRNA distribution fits to a two-component Poisson distribution. Same data set as for the single Poisson distribution. β, fraction of the population with low transcript levels. λ_1, mean transcripts/cell for the fraction of the population with low transcript levels. λ_2, mean transcripts/cell for the fraction of the population with high transcript levels. G test *P* values and ϕ^2 as for single-Poisson fit, but the null hypothesis is that the data have a two-component Poisson distribution with means λ_1 and λ_2.

lower population mRNA means overestimates the number of proteins/transcript. Therefore, we compared the protein abundance to the mRNA means of the high expressing population for the periodic genes (λ_2 from **Table S3**). This results in a linear regression with the same slope as that for the constitutive genes and slightly fewer proteins/mRNA in the group of periodic genes compared with the constitutive genes (**Fig. 4C**)

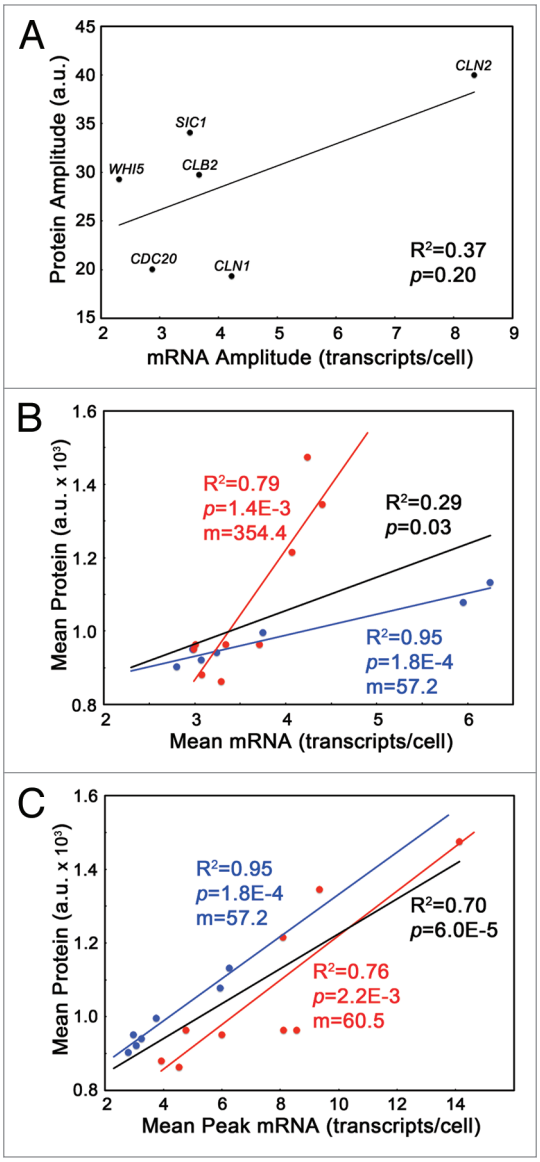

Figure 4. Correlations of mRNA oscillation amplitudes and abundances to protein. Data for all correlation plots is from **Table S3**. All protein data are derived from Ball et al.33 (**A**) Correlation plot for each periodic cell cycle gene showing mRNA amplitudes from FISH experiments ($\lambda_2 - \lambda_1$) compared with protein oscillation amplitudes. Only genes that showed both mRNA and protein oscillations are included. Black line is the linear regression. (**B**) Correlation plot of all 16 cell cycle genes, showing the ratio of the mean transcript abundance from FISH experiments to the mean protein abundance, as measured by fluorescence (mean pixel intensity/cell). The linear regression and statistics for the entire set (black), for the constitutive genes only (blue) and for the periodic genes only (red) are shown. (**C**) Correlation plot of all 16 cell cycle genes. Same as (**B**), except that instead of the mean mRNA abundance for the population, the mean of the high abundance population (λ_2) is used for the periodic genes. R^2 values and *P* values from ANOVA statistical analysis of the linear regressions are shown. Null hypothesis for the *P* value is that there is no correlation between the FISH and protein data.

All of the oscillating proteins in this study are known to be degraded via regulated ubiquitination and the 26S proteasome.[52] Moreover, recent genomic, transcriptomic, and proteomic analyses have found that oscillating cell cycle proteins use sub-optimal codons to regulate translation in conjunction with cell cycle changes in tRNA availability and translation initiation rates.[50,51] Therefore, the lower protein-to-mRNA ratio in periodic genes could be because the oscillating proteins have less efficient translation, enhanced degradation rates, or a combination of both.

These correlations also address the potential for the GFP tag to alter mRNA or protein dynamics. The good agreements of mRNA with protein levels suggest that GFP does not generally affect mRNA or protein synthesis or stability in this set of genes.

Including mRNA in a stochastic model of the cell cycle

We have previously described a multisite phosphorylation model of the budding yeast cell cycle,[11] which accurately recapitulates experimental observations regarding natural variations in cell cycle timing and cell volume (see **Supplementary Material** for a brief description of the model). The model made certain assumptions about the mean levels of mRNA abundances of cell cycle regulators, because at the time there were no data on mRNA abundances in single cells for these genes. In light of our measurements of these mRNA distributions, we decided to revisit the model and assess its predicted mRNA distributions.

First of all, we compared our observed distribution of *CLN2* mRNA (**Fig. 1D**) to our stochastic simulations of MbS (mRNA for G_1/S cyclin *CLBS*) in our original model (Fig. 9B in ref. 10). Our simulations predicted a much larger proportion of cells with high levels of *CLN2* mRNA. To bring the model in line with our observations, we reasoned that the production of *CLN2* mRNA has to be more abrupt, producing a transient peak in abundance to match the observed distribution of *CLN2* mRNA. In order to produce a more abrupt burst of *CLN2* mRNA, we allowed phosphorylation of terminal complex ($CmpP_2$ = complex of $Whi5P_2$ and SBF) by Cln3 and ClbS-dependent kinase, so that $Whi5P_2$ is phosphorylated to $Whi5P_3$, and SBF is released completely from the complex. We also modified the model to allow for phosphorylation of the $RENT_5$ complex, leading to complete release of Cdc14. These simple changes resulted in steeper and more realistic peaks in SBF activity, Cdc14 release, and *CLN2* mRNA (MbS) abundance (compare Fig. 6 to Figs. 3 and 5 in ref. 10).

In addition, the distributions of 2 constitutive mRNAs in our model, *WHI5* and *NET1* transcripts, were shifted slightly to the right compared with our experimental observations. Therefore, to reproduce the observed distributions of *WHI5* and *NET1* transcripts, we reduced the mRNA production rates for these 2 genes and increased protein synthesis rates, such that total protein levels remained the same.

With these small adjustments, the model now captures quantitatively the observed distributions (**Fig. 5**) and quantities (**Table 3**) of *CLN2*, *WHI5*, and *NET1* transcripts and the time-course of expression of the *CLN2* gene (compare **Fig. 6C** to **Fig. S1**). All adjustments to the model are listed in **Tables S3 and S4**.

In addition to fitting the FISH data, simulations of the model with the new parameters corresponded well with the statistics of cell populations collected by Di Talia et al.[14] Examining the timing of G_1 phase, we see a size-dependent component (slope −0.55) for small birth size daughters and a size-independent component (slope −0.22) for larger daughters (**Fig. S4**); the corresponding values in Di Talia et al.[14] are −0.7 and −0.3. In our simulations, the smallest quartile of mother cells show a weak, size-dependent component to the time spent in G_1 (slope −0.18), but most mothers show no size dependence (slope −0.04; **Fig. S4**). Although Di Talia et al.[14] obtained a single straight line with slope −0.1, the small amount of size control in mothers we observe in our new model is a marked improvement over our previous result (slope −0.36).[10,14] Stochastic simulations with our new model produce cell cycle timing and cell volume distributions that correspond well with published observations (**Table 4**). Notice that the greatest variations occur in the timing of G_1, when the number of molecules per cell is lower than in later phases of the cell cycle.

Having incorporated our mRNA observations in the model simulations, we wanted to determine how using the mRNA FISH data affected the outcome of stochastic simulations in comparison to using mRNA abundances reported by microarray studies. We ran simulations and collected statistics for populations in which each cell on average had 4-fold fewer numbers of mRNAs for all the genes included in the model. Although the average properties of cell cycle metrics remain more-or-less the same, the variability of these metrics increases significantly (**Fig. 7**). These results highlight the significance of mRNA levels in determining the amplitude of intrinsic noise and the importance of obtaining absolute mRNA quantities for stochastic modeling of gene expression.

Discussion

Recent attempts to build realistic, accurate, stochastic models of the CDK control system in budding yeast have been hampered by the lack of reliable data on the distribution of transcript numbers for cell cycle control genes in individual yeast cells. Computational models indicated that variability in cell cycle progression is extremely sensitive to the average number of gene transcripts per cell and to the expected half-lives of these mRNA molecules. Data available at the time, from yeast transcriptome studies, suggested that the average number of transcripts per cell was ~1[38] and that mRNA half-lives were ~20 min,[37,38,53] and more recent studies have supported these values.[54,55] Using these numbers, one can easily estimate that fluctuations in protein abundances per cell would be expected to be ± 50–100%, which is likely inconsistent with reliable behavior of any molecular control system.[11]

Later measurements of mRNA transcripts for a handful of non-cell cycle control genes in single yeast cells by fluorescence in situ hybridization (FISH) suggested that the whole-transcriptome measurements might underestimate average mRNA abundances by ~4-fold,[42] and a subsequent microarray study normalized according to this observation gave quantities of transcripts per cell in line with the mRNA FISH measurements.[56] Furthermore, 20 min half-lives for mRNAs involved in cell cycle control seem to be inconsistent with how fast gene expression is turned on and off during normal cell cycle progression and in response to regulated promoters. In general, transcripts encoding regulatory proteins have shorter mean half-lives than transcripts coding for central metabolic proteins.[37] More specifically, recent transcriptome analyses indicate that the transcripts for cell cycle genes compose a large proportion of the least stable transcripts.[54] In fact, the half-lives for the 16 cell cycle genes included in the current study fall in the range of 5–10 min when measured by Dynamic Transcriptome Analysis (**Table S1**).[54,56]

To help resolve uncertainties in mRNA quantities, we set out to measure the absolute quantities and distributions of mRNA transcripts of 16 cell cycle control genes in single yeast cells by FISH. Our data confirmed that the whole-transcriptome estimates are too low by ~4-fold. In addition, we were able to extract information about the dynamics of gene expression from a "snapshot" of the mRNA distribution in an asynchronous culture of yeast cells. Constitutive genes fit a single Poisson distribution, while periodic genes generally fit a two-component Poisson distribution. The low *P* values for some constitutive genes using the Poisson model (e.g., *MCM1*) and also some periodic genes for the two-component Poisson model (e.g., *CLN1*) suggest that these distributions may not fit the observed data exactly. However, the effect sizes (ϕ^2 in **Table 1**; **Table S1**), Q–Q plots (**Fig. S2**), and density overlays (**Fig. 1**) suggest that the one- and two-component Poisson models generally fit the constitutive and periodic data well. Nevertheless, our observations that the mRNA distributions for some genes do not exactly fit single or two-component Poisson distributions might be a consequence of using an oversimplified two-state model for transcription.

Comparisons between mRNA and protein also yielded some interesting observations. We found that transcript periodicity corresponds to protein oscillations, and that constitutively transcribed genes usually produce constitutive protein levels. These might appear to be obvious correlations, but it is theoretically possible that a constitutively transcribed gene could produce protein oscillations via post-transcriptional mechanisms, or that these same mechanisms could also smooth out mRNA periodicity to yield constitutive protein levels. These 2 situations could arise in response to rapid developmental/environmental changes or as evolutionary intermediates as a gene is utilized for a new function, but we are not likely to see discordant mRNA and protein regulation during exponential growth in such ancient regulatory networks as those controlling the cell cycle.

Table 3. mRNA quantities from stochastic simulations of the model compared with observed quantities

Gene	Mean[a]		CV[b]	
	Model	Expt	Model	Expt
CLBS	6.2	4.5	1.19	1.14
NET1	6.8	6.2	0.21	0.43
WHI5	4.2	3.5	0.49	0.67

[a]Data from the biological replicates shown in **Table 1**. Similar results are obtained with all replicates; [b]Coefficients of variation (CV = standard deviation/mean).

Table 4. Population statistics of stochastic simulations compared with experimental values[14]

Quantity[a]	Daughter cell				Mother cell			
	Mean (model)	Mean (expt)	CV[b] (model)	CV (Expt)	Mean (model)	Mean (expt)	CV (model)	CV (expt)
T_{div}	118.0	112.0	0.18	0.22	91.3	87.0	0.20	0.14
T_{G1}	40.6	37.0	0.43	0.50	13.5	16.0	0.47	0.50
T_{SG2M}	77.5	76.0	0.21	0.20	77.8	72.0	0.23	0.17
V_{birth}	31.3	28.0	0.29	0.22	46.9	40.0	0.29	0.18
V_{div}	70.9		0.25		89.1		0.30	

[a]T_{div}, time from birth to division; T_{G1}, time from birth to bud formation; T_{SG2M}, time from bud formation to division; V_{birth}, daughter cell volume at birth; V_{div}, mother cell volume at division; [b]Coefficients of variation (CV = standard deviation/mean).

Although there was no significant correlation between the amplitudes of mRNA and protein oscillations, mRNA abundances agreed very well with protein abundances. For constitutively expressed genes and periodic genes, the mean abundances of mRNA and protein correlated well, but only when grouped separately. On the other hand, using the transcript abundance of the high-expressing population (λ_2) produced a correlation for periodic genes that fit well with the constitutive genes. These observations demonstrate one of the caveats of transcriptome–proteome correlations—using population means produces a poor mRNA-protein correlation when combining constitutive and regulated genes in the analysis, which is why various methodologies, such as principal component analysis, must be used to identify groups of differently regulated genes.

Three genes (*ESP1*, *TEM1*, and *WHI5*) that Cyclebase labels as periodic exhibit mRNA distributions that are marginally fit by a single Poisson distribution. Examining their expression profiles in Cyclebase (see **Fig. S1**), we find that the data are quite noisy, that the changes in transcript abundance are quite small (~2-fold ratio between λ_1 and λ_2), and that the majority of cells are grouped in the higher abundance population ($\beta < 0.5$), reflecting their broad peaks of expression (**Table 1; Table S1**). Furthermore, in a previous study, we similarly found the Esp1 and Tem1 proteins do not show significant oscillations.[33] Although these genes may indeed be weakly periodic, modeling their expression as constitutive produced an excellent fit of our simulations to the available experimental data. In addition, when performing mRNA–protein comparisons, it made no significant difference if we grouped *ESP1*, *TEM1*, and *WHI5* with constitutive genes or with periodic genes (data not shown).

Using these measurements of mRNA distributions of cell cycle control genes, we were able to significantly improve our published model of the budding yeast cell cycle.[10] The observed distributions of *CLN1* and *CLN2* transcripts suggested a major change in how

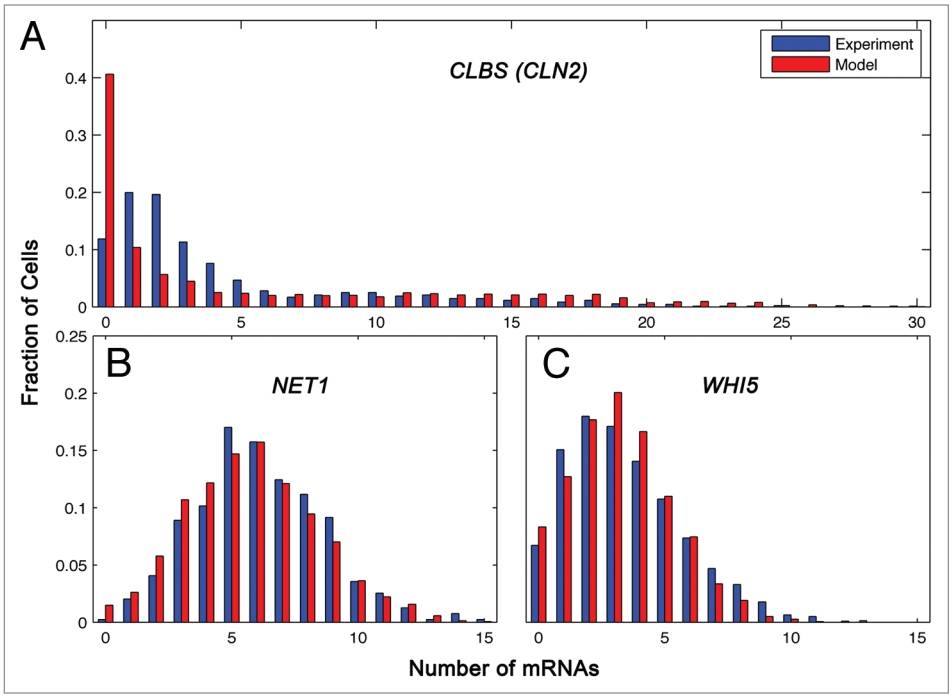

Figure 5. mRNA distributions from stochastic simulations of the model compared with observed distributions. (**A–C**) Comparison of experimentally observed mRNA abundance to simulated distributions for (**A**) *CLN2*, (**B**) *NET1*, and (**C**) *WHI5*. Experimental data are from biological replicates shown in **Table 1**. Similar results are obtained with all biological replicates.

we modeled the phosphorylation of Whi5:SBF complexes and of Net1:Cdc14 complexes. The observed distributions of other genes prompted minor changes in the rate constant values for gene transcription and translation. After these changes were made, not only was our model brought into alignment with our measured gene expression profiles, but also it was more successful in fitting the observed distributions of other cell cycle metrics. Although the mRNA half-lives used in this model (1–5 min) are shorter than measured values (5–10 min),[54,56] the discrepancy might easily be accounted for by some degree of mRNA gestation and senescence, as explained in the supplement to Barik et al.[10] A new version of the model (under development), will include periodic expression of *CLB2, SIC1, CDC6*, and *CDC20*, using the data collected here to determine the correct mRNA distributions in the model. Furthermore, mRNA half-lives in the new model (2–10 min) are more in line with the best recent measurements.[54,56]

Our results show the benefits of absolute quantification of molecules in single cells. Because our approach counts mRNA molecules, we avoid the pitfalls of converting inherently relative data to absolute quantities by an intrinsically uncertain normalization factor. Remarkably, in addition to the benefits of having single-cell mRNA abundance measurements for mathematical modeling of gene expression, this data also provided insights into the dynamics of gene expression during cell cycle progression. We were able to determine if genes were constitutively expressed or regulated, and for the regulated genes, we were able to deduce the fraction of cell cycle time in which these genes are expressed and the magnitude of change in expression—all from analysis of static mRNA distributions in unperturbed asynchronous cells.

Although our experimental design precluded us from correlating transcript numbers to cell cycle phase, asynchronous cells can be staged using morphological markers such as the presence of a bud, myosin and/or Whi5 localization, and microtubule structures.[14,57] Including such markers in automated analyses and correlating transcript numbers using 2-color FISH[42] or fluorescent protein labeling of mRNA[58] could produce high-definition data sets that include quantitative temporal information on single-cell behavior, for hypothesis testing and stochastic modeling of gene expression networks.

Materials and Methods

Yeast strains and media

Each *S. cerevisiae* strain used in this study included GFP inserted as an in-frame C-terminal fusion with a gene involved in cell cycle control.[59] All strains were purchased from Invitrogen. Strains were tested for correct integration of the GFP tag by PCR-amplification of genomic DNA and growth characteristics, and protein dynamics were normal, suggesting that the fusions were functional.[33] Cells were grown to an OD_{600} of 0.4 in synthetic complete (SC) growth medium with 2% glucose at 30 °C prior to fixation and hybridization of probes.

Cell cycle analysis

For cell cycle synchronization experiments with the *CLN2-GFP* strain, cells were grown as described above and arrested in G_1 by the addition of 20 μM α-factor. Cell cycle arrest was monitored by removing 500 μL of culture, sonicating the cells (Branson Sonifier with microprobe, 10 s at power setting 4), and observing cells under differential interference contrast (DIC) microscopy until >95% of cells are unbudded with a small mating projection (~60 min). To release the cells from arrest, cells were harvested by centrifugation, washed once in sterile water, and resuspended in warm SC medium.

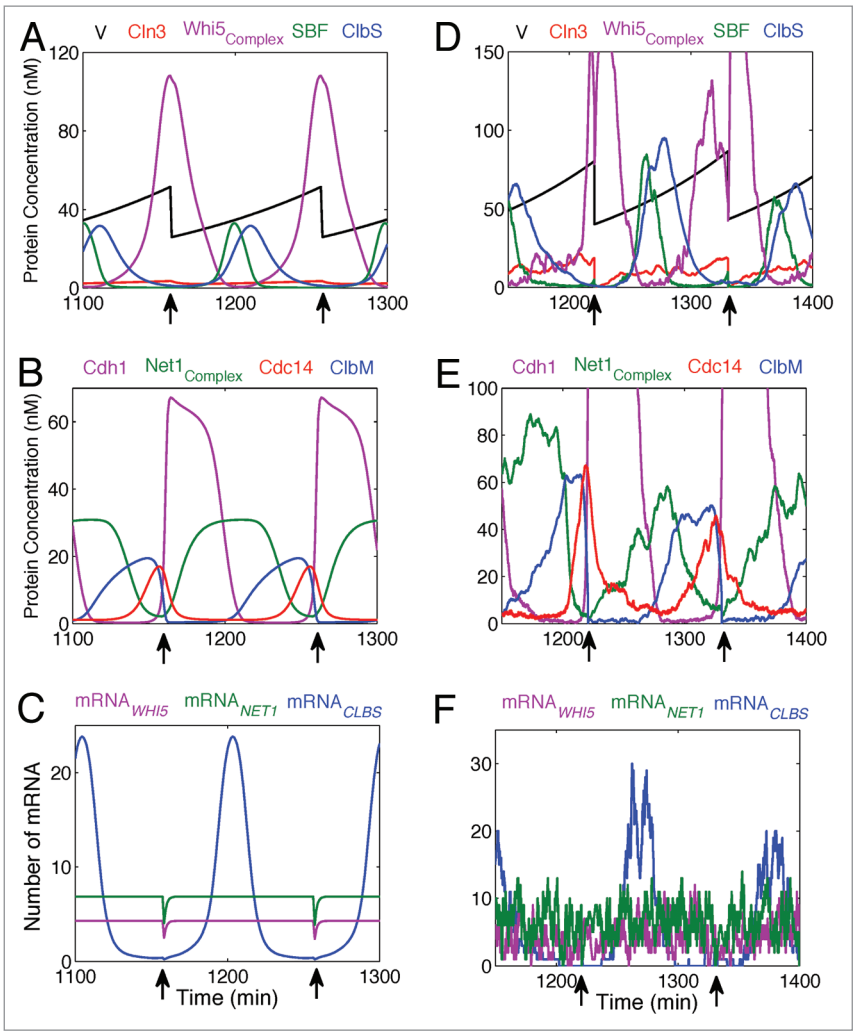

Figure 6. Oscillatory dynamics of key proteins and mRNAs of the model. (**A–C**) Deterministic simulations of the model showing time-course plots of protein concentrations (**A and B**) and mRNA abundances (**C**). (**D–F**) Stochastic trajectories of the same species are shown as in panels (**A–C**). In deterministic simulations, cell volume is divided equally at cell division (indicated by the arrows at the bottom of each plot). In stochastic simulations, cell volume is divided 60:40 (mother:daughter) at cell division.

At various time points before and after synchronization, we removed a 60 mL sample with 50 mL to be processed for FISH, as described below, and 10 mL to be processed for fluorescence-activated cell sorting (FACS) analysis of DNA content and for bud morphology analysis (budding index). The 10 mL sample was centrifuged and washed twice in sterile nuclease-free water. The cell pellet, consisting of approximately 2 x 10^8 cells, was resuspended in 1 mL of water and divided equally into 2 micro-centrifuge tubes. The cells were sonicated, and an equal volume of absolute ethanol was added to fix the cells, which were stored at 4 °C overnight (or longer). Fixed cells were washed twice in sterile nuclease-free water before processing for FACS or budding index.

Samples for budding index analysis were resuspended in 1 mL of sterile nuclease-free water and stained with 2 µg/mL final concentration of Hoechst 33342 (Invitrogen, http://products.invitrogen.com/ivgn/product/H1399) for 2 h. Cells were then briefly sonicated, washed once in sterile nuclease-free water, and wet-mounted on slides for observation on a fluorescence microscope as described below except that single focus images were acquired. After acquisition, image files in TIFF format were automatically converted to Omero files and uploaded to an image storage server using Omero Insight's importer.[60] We used composite images of the phase-contrast and Hoechst channels to score unbudded G_1 cells, small-budded S-phase cells in which the bud is <1/3 the size of the mother, large-budded G_2/M cells with a single aggregate of DNA (nucleus), and large-budded anaphase/telophase cells with an elongated nucleus in the mother-bud neck or with mother and bud both containing a single nucleus, respectively.

Samples for FACS analysis of DNA content were sonicated, pelleted, and resuspended in 1 mL of RNase A (Sigma-Aldrich) solution (50 mM Tris-CL, pH 8.0, 15 mM NaCl, 2 mg/mL RNase A), and incubated at 37 °C for 4 h.[61] After incubation, proteinase K (New England Biolabs) was added directly to the solution to a final concentration of 200 µg/mL, and the tube was incubated at 37 °C for a further 1 h. Cells were then centrifuged, resuspended in 50 mM Tris-Cl, pH 8.0, and stained for immediate FACS analysis or stored at 4 °C. DNA staining was accomplished by adding 100 µL of cells to 1 mL of SYTOX green (Invitrogen, http://products.invitrogen.com/ivgn/product/S7020) solution (1 µM SYTOX Green in 50 mM Tris-Cl, pH 8.0). The stained cells were briefly sonicated, and FACS analysis was performed on a BD LSR II using the Argon laser

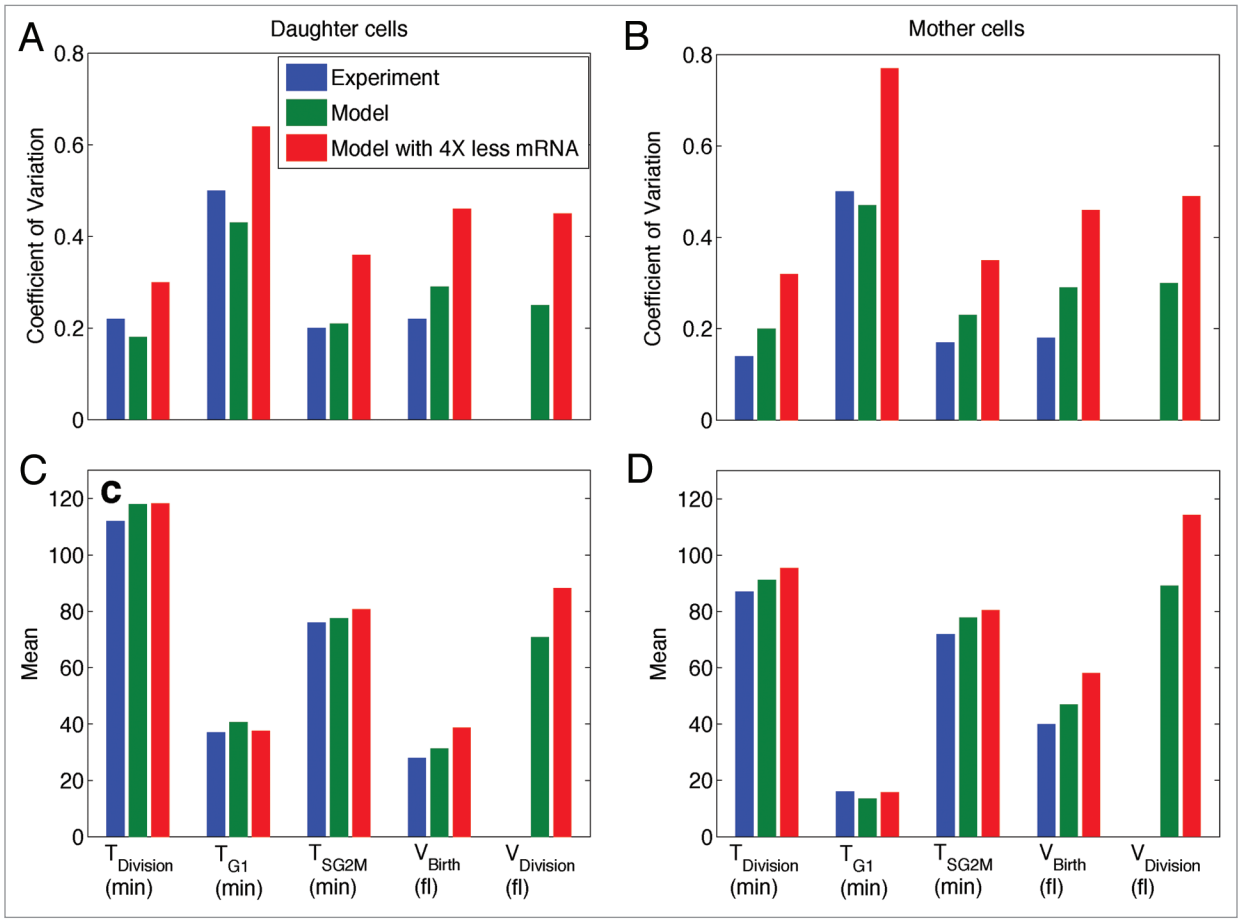

Figure 7. Low mRNA abundance increases cell cycle variability. In these 4 panels we compare the means and coefficients of variation (CV, standard deviation/mean) of 5 cell cycle metrics (T_{Div}, interdivision time; T_{G1}, duration of unbudded phase; T_{SG2M}, duration of budded phase; V_{Birth}, size at birth; $V_{Division}$, size at division) for mother cells and daughter cells. Blue bars, experimental measurements (from ref. 14); green bars, model simulations as described in the text; red bars, model simulations with 4-fold reduction in the average numbers of transcripts of all genes in the model.

(488 nm) and FITC filter (505 LP splitter and 525/50 BP filter). Data was collected and analyzed with BD FACSDiva 7.0.

FISH probes

Five, 50mer oligonucleotides were designed to target the GFP moiety of mRNA transcribed from the GFP-tagged genes (**Supplementary Methods**; **Table 1**). The oligos were synthesized commercially (BioSearch Technologies), and each oligo contained 5 modified Ts that carried an amino group. A DyeLight 550 NHS Ester labeling kit (Thermo Scientific, http://www.piercenet.com/browse.cfm?fldID=E3F90446-A514-E35F-2A86-0F053949F201) was used to conjugate the fluorescent dye DyeLight 550 to the modified Ts.

List of oligonucleotides used in this study

See **Table 5**.

Hybridization

Hybridization was performed as described.[42] Briefly, cells were first fixed by incubation in 4% (v/v) paraformaldehyde (Electron Microscopy Sciences, http://www.emsdiasum.com/microscopy/products/chemicals/formaldehyde.aspx) for 45 min. After washing 3 times in Buffer B (1.2 M Sorbitol, 100 mM $KHPO_4$, pH 7.5), cells were resuspended in spheroplast buffer (1.2 M Sorbitol, 100 mM $KHPO_4$ pH 7.5), 20 mM Ribonucleoside-Vanadyl complex (New England Biolabs, https://www.neb.com/products/s1402-ribonucleoside-vanadyl-complex), 20 mM β-mercaptoethanol, and 25 U lyticase (Sigma-Aldrich, http://www.sigmaaldrich.com/catalog/product/sigma/l2524), and incubated at 30 °C for 7 min to partially digest the cell walls. Cells were placed on poly-L-lysine (Sigma-Aldrich) coated coverslips and allowed to settle for 30 min at 4 °C. The coverslips were washed once with Buffer B to remove unattached cells and stored overnight in 70% ethanol. The ethanol was removed, and the coverslips were incubated twice in 2× saline-sodium citrate (SSC) for 5 min and once in 40% formamide/2× SSC. Coverslips were then incubated with a mixture of the 5 probes (0.4 ng each, 2 ng total) overnight at 37 °C. Unbound probe was removed by washing the coverslips twice with 40% formamide/2× SSC, once with 2× SSC/0.1% Triton, and once with 1× SSC. The coverslips were then washed in a Hoechst 33342 solution to stain nuclei and mounted on slides with Prolong Gold mounting medium (Life Technologies, http://products.invitrogen.com/ivgn/product/P36930).

Imaging

All images were collected on an Axio Observer Z1 (Zeiss, http://microscopy.zeiss.com/microscopy/en_de/products/imaging-systems/cell-observer.html) microscope equipped with a CoolSNAP *HQ*^{2} CCD camera (Photometrics, http://www.photometrics.com/products/ccdcams/coolsnap_hq2.php), a halogen lamp for bright field imaging, and a 120 W metal halide lamp for fluorescence excitation. The microscope is controlled by custom software developed in MATLAB that relies on the API of the open-source microscopy control software, μManager.[62] The custom software performs image-processing tasks during acquisition and, among other features, allows for the automatic identification of suitable fields of view (FOVs); therefore, maximizing the number of cells that can be sampled. For each strain, 20 FOVs, containing ~1000 cells in total, were automatically selected from a user-defined area of the slide. A z-stack was collected at each FOV containing 31 focal planes separated by 0.2 μm, and 2 color channels: DyeLight 550 (Chroma filter set SP102v1, exposure time: 2 s/plane), and Hoechst 33342 (Chroma filter set 49 000, exposure time: 150 ms/plane). In addition, a single phase-contrast image was acquired at the central plane for automated cell identification (see below).

Image processing

Phase-contrast images were segmented using custom software derived from Yeast Tree 1.6.3.[15] The application relies on the MATLAB Image Processing toolbox. First, the function "imfill" was used to flood-fill local minima not connected to the image border, which fills in the center of the groups of cells. As each group of cells has slightly different levels to which the flood-fill will rise, we then searched the image histogram for intensities greater than the calculated background, taken from the border pixels, and with a frequency greater than the minimum cell area, generally set to 200 pixels. To keep only large groups of connected pixels, erosion (built-in function "imerode") was performed, removing the outermost pixels of a region and eliminating small groups of pixels.

The next step is to separate these groups into individual cells. This was done with another call to "imerode" to cut the small necks that appear between touching cells. Once the cells are cut, the remaining connected regions were labeled with a call to the built-in function "bwlabel", which identifies the individual cells and assigns each with a unique label. To finish, the cells were returned to their original sizes with a dilation (built-in function "imdilate"), which adds pixels around the edges of each cell.

Prior to the identification of spots, the 3-dimensional fluorescence z-stacks were reduced to 2D images by use of a maximum z-projection. Single spots, corresponding to mRNA molecules, were then identified using the algorithm described.[41] First, a local background subtraction, in which the mean of a 19 × 19 pixel neighborhood is subtracted from the central pixel, was used to highlight the bright punctate spots from the autofluorescence

Table 5. List of oligonucleotides used in this study

Probe ID	Sequence[a]
GFP 70	**T**CCGTATGT**T** GCATCACCT**T** CACCCTCTCC AC**T**GACAGAA AATTTG**T**GCCC
GFP 304	GGG**T**ATCACC TTCAAAC**T**TG ACTTCAGCAC G**T**GTCTTGTAG **T**TCCCGTCA**T**C
GFP 555	**T**GGACAGGTA A**T**GGTTGTCT GG**T**AAAAGGA CAGGGCCA**T**C GCCAATTGGA G**T**A
GFP 628	GCAGC**T**GTTA CAAAC**T**CAAG AAGGACCA**T**G TGGTCTCTC**T** TTTCGTTGGG A**T**C
GFP 682	**T**AGAAGTGGC GCGCCC**T**ATT TGTATAG**T**TC ATCCATGCCA **T**GTGTAATC**T**C

[a]Nucleotides in bold are modified with amino groups for conjugation to a fluorophore.

background of the cells. Then, pixels 5 standard deviations above the mean pixel value of the entire image were chosen as initial seeds for the spot detection routine. Gaussian weighting was then used to move each seed to the center of the 2D Gaussian intensity distribution. Spots with an integrated intensity of <350 are likely the result of non-specifically bound individual probes and were therefore removed. Finally, to avoid double counting a single mRNA, if the centers of 2 spots were within 2 pixels of each other, then the dimmer of the 2 spots was removed.

Microarray data analysis

Microarray-derived relative gene expression data sets for each cell cycle gene were downloaded from Cyclebase.[46] These data sets represent 6 independent time-course microarray experiments performed using synchronized budding yeast cell cultures.[44,45,47,48] Because these data sets are from cells synchronized at different points in the cell cycle, Cyclebase provides them in a form in which all the experiments are time-registered to start at the same point in the cell cycle— roughly, late M/G_1. Since the time points were different for the various experiments, we used the MATLAB cubic spline interpolation function to obtain high-resolution (0.001 min intervals) data sets for each experiment. We then obtained the means for 16 common time points (12 min intervals—the same as Spellman et al.[48]) across the 6 data sets and performed a cubic spline interpolation (0.001 min intervals) of the mean expression levels to plot the mean expression profiles over the course of 2 cell cycles (**Fig. S1**). These mean values were used for comparisons to the single mRNA FISH data.

Statistical analysis

The transcription of constitutively expressed genes was assumed to be the result of a random birth and death process with exponentially distributed waiting times. To characterize variability between experimental replicates, the following analyses were conducted on each experimental replicate separately. We used maximum-likelihood estimation to compare the distributions of mRNAs in unsynchronized populations to a single component Poisson function, with probability density function (PDF) defined as:

(1), $$P_1(x) = \frac{\lambda_1^x e^{-\lambda_1}}{x!}$$

where λ is the mean of the Poisson distribution.

For regulated genes, we assumed that our population includes 2 groups: one group of cells transcribing the gene at the low rate, and the other transcribing at a high rate. We make the further assumption that transcription in both groups has reached steady state, and so using maximum-likelihood estimation, the distribution was compared with a two-component Poisson with PDF:

(2), $$P_2(x) = \beta \frac{\lambda_1^x e^{-\lambda_1}}{x!} + (1-\beta)\frac{\lambda_2^x e^{-\lambda_2}}{x!}$$

where λ_1 and λ_2 are the means of the mRNA abundance in the 2 transcription states, and β is the proportion of cells with the lower mean transcript abundance (λ_1), $0 \le \beta \le 1$.

To determine if the experimental distributions, *O(x)*, were adequately described by these distribution functions, we used likelihood ratio goodness of fit hypothesis tests, ϕ^2 measures of effect size, and quantile-quantile plots.

The goodness of fit test statistic is:

$$G = 2\sum_i O_i \ln\left(O_i / E_i\right)$$

where $i = 1,\ldots,k$ indexes the number of observed outcomes, and O_i and E_i represent the number of observed and expected counts for each outcome. To satisfy the asymptotic assumptions of this test, outcomes which had few counts were binned together, such that $E_i > 5$ in all cases. Under the hypothesis that the observed data arise from the theoretical distribution, G has an asymptotic Chi-square distribution with $k - p - 1$ degrees of freedom, where k is the number of data points, and p is the number of parameters estimated from the data ($p = 1$ for the Poisson model and $p = 3$ for the two-component Poisson model). The P value for this hypothesis test is calculated as the upper tail of the appropriate Chi-square distribution.

The measure of effect size ϕ^2 is:

$$\phi^2 = \frac{1}{n}\sum_i \frac{(O_i - E_i)^2}{E_i}$$

where n is the sample size for a given gene. This measure summarizes the average normalized squared deviation between the number of observations in a cell and the number expected under a postulated model. Effect size conventions proposed by Cohen (1988) were used to classify small, medium, and large effects.[63]

Quantile–quantile (Q–Q) plots (**Fig. S2**) were created by plotting the observed quantiles of the data against the corresponding theoretical quantiles of the proposed models. If data truly arise from the proposed model, then the points on the Q–Q plot will adhere closely to the $X = Y$ line. Since these data and the corresponding models take non-negative integer values, a small amount of random noise was added (also known as jittering) to enhance visibility in the Q–Q plots.

Modeling

The model presented here is nearly identical to that described in Barik et al.[10] with some exceptions noted in the modeling section of the results and listed in **Tables S3 and S4**. Deterministic simulations were performed in MATLAB using the ode15s solver. In deterministic simulations, we triggered cell division whenever ClbM concentration level drops below 12.5 nM as the cell exits mitosis. At cell division, cell volume is distributed to mother and daughter cells in a 60:40 ratio,[14] but protein concentrations are unchanged.

Stochastic simulations were performed using Gillespie SSA.[35] In stochastic simulations (as in the deterministic case), cell division occurs whenever ClbM concentration drops below 12.5 nM. To avoid multiple divisions caused by ClbM concentration fluctuating back and forth across 12.5 nM, we insist that ClbM concentration must increase above 20 nM before a subsequent division can be triggered by falling ClbM concentration. We use a pseudo-steady-state approximation for activation of the *CLBS* gene, under the assumption that SBF binds to and dissociates from the *CLBS* gene very rapidly. At cell division, we partitioned cell volume and all molecular species to the mother and daughter cells in a 60:40 ratio, except for Cln3, which was apportioned 75% to the mother cell and 25% to the daughter cell. This rule was intended to account for the fact that *CLN3* expression in

newborn daughters is 1/3 that of newly divided mother cells due to repression of *CLN3* by Ace2 and Ash1.[64]

In stochastic simulations, we followed both mother and daughter cells to generate a complete pedigree of growing and dividing cells. For each cell, we recorded T_{G1} = time from birth to onset of DNA synthesis (when ClbS rises above 25 nM) and T_1 = time from birth to Start (when SBF rises above 15 nM).

Disclosure of Potential Conflicts of Interest

No potential conflicts of interest were disclosed.

Acknowledgments

We are grateful to Daniel Zenklusen for generously providing advice in setting up FISH experiments, to Patrick Cramer and Björn Schwalb for providing published cDTA data, to Adria Carbo for help with FACS analysis, and to Matt Lux for helpful discussions. This project was supported by grants R01-GM078989 and R01-GM095955 from the National Institutes of Health. The funders had no role in study design, data collection and analysis, decision to publish, or preparation of the manuscript.

Author Contributions

DAB designed and performed the experiments, collected the data, analyzed the data, and wrote the manuscript. NRA designed and performed the experiments, collected the data, analyzed the data, and wrote the manuscript. NR performed the experiments and collected the data. DB performed the modeling and simulations. CF analyzed the data. JT designed the experiments, analyzed the data, and wrote the manuscript. JP designed the experiments, analyzed the data, and wrote the manuscript.

Supplemental Materials

Supplemental materials may be found here:
www.landesbioscience.com/journals/cc/article/26257

References

1. Howell AS, Lew DJ. Morphogenesis and the cell cycle. Genetics 2012; 190:51-77; PMID:22219508; http://dx.doi.org/10.1534/genetics.111.128314
2. Barberis M. Sic1 as a timer of Clb cyclin waves in the yeast cell cycle--design principle of not just an inhibitor. FEBS J 2012; 279:3386-410; PMID:22356687; http://dx.doi.org/10.1111/j.1742-4658.2012.08542.x
3. Uhlmann F, Bouchoux C, López-Avilés S. A quantitative model for cyclin-dependent kinase control of the cell cycle: revisited. Philos Trans R Soc Lond B Biol Sci 2011; 366:3572-83; PMID:22084384; http://dx.doi.org/10.1098/rstb.2011.0082
4. Segal M. Mitotic exit control: a space and time odyssey. Curr Biol 2011; 21:R857-9; PMID:22032192; http://dx.doi.org/10.1016/j.cub.2011.09.023
5. McInerny CJ. Cell cycle regulated gene expression in yeasts. Adv Genet 2011; 73:51-85; PMID:21310294; http://dx.doi.org/10.1016/B978-0-12-380860-8.00002-1
6. Munsky B, Neuert G, van Oudenaarden A. Using gene expression noise to understand gene regulation. Science 2012; 336:183-7; PMID:22499939; http://dx.doi.org/10.1126/science.1216379
7. Swain PS, Elowitz MB, Siggia ED. Intrinsic and extrinsic contributions to stochasticity in gene expression. Proc Natl Acad Sci U S A 2002; 99:12795-800; PMID:12237400; http://dx.doi.org/10.1073/pnas.162041399
8. Ball DA, Ahn TH, Wang P, Chen KC, Cao Y, Tyson JJ, Peccoud J, Baumann WT. Stochastic exit from mitosis in budding yeast: model predictions and experimental observations. Cell Cycle 2011; 10:999-1009; PMID:21350333; http://dx.doi.org/10.4161/cc.10.6.14966
9. Lu Y, Cross FR. Periodic cyclin-Cdk activity entrains an autonomous Cdc14 release oscillator. Cell 2010; 141:268-79; PMID:20403323; http://dx.doi.org/10.1016/j.cell.2010.03.021
10. Barik D, Baumann WT, Paul MR, Novak B, Tyson JJ. A model of yeast cell-cycle regulation based on multisite phosphorylation. Mol Syst Biol 2010; 6:405; PMID:20739927; http://dx.doi.org/10.1038/msb.2010.55
11. Kar S, Baumann WT, Paul MR, Tyson JJ. Exploring the roles of noise in the eukaryotic cell cycle. Proc Natl Acad Sci U S A 2009; 106:6471-6; PMID:19246388; http://dx.doi.org/10.1073/pnas.0810034106
12. Tyson JJ, Diekmann O. Sloppy size control of the cell division cycle. J Theor Biol 1986; 118:405-26; PMID:3520151; http://dx.doi.org/10.1016/S0022-5193(86)80162-X
13. Skotheim JM, Di Talia S, Siggia ED, Cross FR. Positive feedback of G1 cyclins ensures coherent cell cycle entry. Nature 2008; 454:291-6; PMID:18633409; http://dx.doi.org/10.1038/nature07118
14. Di Talia S, Skotheim JM, Bean JM, Siggia ED, Cross FR. The effects of molecular noise and size control on variability in the budding yeast cell cycle. Nature 2007; 448:947-51; PMID:17713537; http://dx.doi.org/10.1038/nature06072
15. Bean JM, Siggia ED, Cross FR. Coherence and timing of cell cycle start examined at single-cell resolution. Mol Cell 2006; 21:3-14; PMID:16387649; http://dx.doi.org/10.1016/j.molcel.2005.10.035
16. Cokus S, Rose S, Haynor D, Grønbech-Jensen N, Pellegrini M. Modelling the network of cell cycle transcription factors in the yeast Saccharomyces cerevisiae. BMC Bioinformatics 2006; 7:381; PMID:16914048; http://dx.doi.org/10.1186/1471-2105-7-381
17. Bosl WJ, Li R. Mitotic-exit control as an evolved complex system. Cell 2005; 121:325-33; PMID:15882616; http://dx.doi.org/10.1016/j.cell.2005.04.006
18. Cross FR, Archambault V, Miller M, Klovstad M. Testing a mathematical model of the yeast cell cycle. Mol Biol Cell 2002; 13:52-70; PMID:11809822; http://dx.doi.org/10.1091/mbc.01-05-0265
19. López-Avilés S, Kapuy O, Novák B, Uhlmann F. Irreversibility of mitotic exit is the consequence of systems-level feedback. Nature 2009; 459:592-5; PMID:19387440; http://dx.doi.org/10.1038/nature07984
20. Pomerening JR, Sontag ED, Ferrell JE Jr. Building a cell cycle oscillator: hysteresis and bistability in the activation of Cdc2. Nat Cell Biol 2003; 5:346-51; PMID:12629549; http://dx.doi.org/10.1038/ncb954
21. Sha W, Moore J, Chen K, Lassaletta AD, Yi CS, Tyson JJ, Sible JC. Hysteresis drives cell-cycle transitions in Xenopus laevis egg extracts. Proc Natl Acad Sci U S A 2003; 100:975-80; PMID:12509509; http://dx.doi.org/10.1073/pnas.0235349100
22. Yao G, Tan C, West M, Nevins JR, You L. Origin of bistability underlying mammalian cell cycle entry. Mol Syst Biol 2011; 7:485; PMID:21525871; http://dx.doi.org/10.1038/msb.2011.19
23. Charvin G, Cross FR, Siggia ED. Forced periodic expression of G1 cyclins phase-locks the budding yeast cell cycle. Proc Natl Acad Sci U S A 2009; 106:6632-7; PMID:19346485; http://dx.doi.org/10.1073/pnas.0809227106
24. Cross FR, Schroeder L, Kruse M, Chen KC. Quantitative characterization of a mitotic cyclin threshold regulating exit from mitosis. Mol Biol Cell 2005; 16:2129-38; PMID:15716353; http://dx.doi.org/10.1091/mbc.E04-10-0897
25. Chen KC, Calzone L, Csikasz-Nagy A, Cross FR, Novak B, Tyson JJ. Integrative analysis of cell cycle control in budding yeast. Mol Biol Cell 2004; 15:3841-62; PMID:15169868; http://dx.doi.org/10.1091/mbc.E03-11-0794
26. Sveiczer A, Tyson JJ, Novak B. A stochastic, molecular model of the fission yeast cell cycle: role of the nucleocytoplasmic ratio in cycle time regulation. Biophys Chem 2001; 92:1-15; PMID:11527575; http://dx.doi.org/10.1016/S0301-4622(01)00183-1
27. Steuer R. Effects of stochasticity in models of the cell cycle: from quantized cycle times to noise-induced oscillations. J Theor Biol 2004; 228:293-301; PMID:15135028; http://dx.doi.org/10.1016/j.jtbi.2004.01.012
28. Singhania R, Sramkoski RM, Jacobberger JW, Tyson JJ. A hybrid model of mammalian cell cycle regulation. PLoS Comput Biol 2011; 7:e1001077; PMID:21347318; http://dx.doi.org/10.1371/journal.pcbi.1001077
29. Zhang YP, Qian MP, Ouyang Q, Deng MH, Li FT, Tang C. Stochastic model of yeast cell-cycle network. Physica D 2006; 219:35-9; http://dx.doi.org/10.1016/j.physd.2006.05.009
30. Okabe Y, Sasai M. Stable stochastic dynamics in yeast cell cycle. Biophys J 2007; 93:3451-9; PMID:17704157; http://dx.doi.org/10.1529/biophysj.107.109991
31. Braunewell S, Bornholdt S. Superstability of the yeast cell-cycle dynamics: ensuring causality in the presence of biochemical stochasticity. J Theor Biol 2007; 245:638-43; PMID:17204290; http://dx.doi.org/10.1016/j.jtbi.2006.11.012
32. Ge H, Qian H, Qian M. Synchronized dynamics and non-equilibrium steady states in a stochastic yeast cell-cycle network. Math Biosci 2008; 211:132-52; PMID:18048065; http://dx.doi.org/10.1016/j.mbs.2007.10.003
33. Ball DA, Marchand J, Poulet M, Baumann WT, Chen KC, Tyson JJ, Peccoud J. Oscillatory dynamics of cell cycle proteins in single yeast cells analyzed by imaging cytometry. PLoS One 2011; 6:e26272; PMID:22046265; http://dx.doi.org/10.1371/journal.pone.0026272

34. Charvin G, Oikonomou C, Siggia ED, Cross FR. Origin of irreversibility of cell cycle start in budding yeast. PLoS Biol 2010; 8:e1000284; PMID:20087409; http://dx.doi.org/10.1371/journal.pbio.1000284
35. Gillespie DT. General Method for Numerically Simulating Stochastic Time Evolution of Coupled Chemical-Reactions. J Comput Phys 1976; 22:403-34; http://dx.doi.org/10.1016/0021-9991(76)90041-3
36. Sabouri-Ghomi M, Ciliberto A, Kar S, Novak B, Tyson JJ. Antagonism and bistability in protein interaction networks. J Theor Biol 2008; 250:209-18; PMID:17950756; http://dx.doi.org/10.1016/j.jtbi.2007.09.001
37. Wang Y, Liu CL, Storey JD, Tibshirani RJ, Herschlag D, Brown PO. Precision and functional specificity in mRNA decay. Proc Natl Acad Sci U S A 2002; 99:5860-5; PMID:11972065; http://dx.doi.org/10.1073/pnas.092538799
38. Holstege FC, Jennings EG, Wyrick JJ, Lee TI, Hengartner CJ, Green MR, Golub TR, Lander ES, Young RA. Dissecting the regulatory circuitry of a eukaryotic genome. Cell 1998; 95:717-28; PMID:9845373; http://dx.doi.org/10.1016/S0092-8674(00)81641-4
39. Zenklusen D, Singer RH. Analyzing mRNA expression using single mRNA resolution fluorescent in situ hybridization. Methods Enzymol 2010; 470:641-59; PMID:20946829; http://dx.doi.org/10.1016/S0076-6879(10)70026-4
40. Peccoud J, Ycart B. Markovian Modeling of Gene-Product Synthesis. Theor Popul Biol 1995; 48:222-34; http://dx.doi.org/10.1006/tpbi.1995.1027
41. Thompson RE, Larson DR, Webb WW. Precise nanometer localization analysis for individual fluorescent probes. Biophys J 2002; 82:2775-83; PMID:11964263; http://dx.doi.org/10.1016/S0006-3495(02)75618-X
42. Zenklusen D, Larson DR, Singer RH. Single-RNA counting reveals alternative modes of gene expression in yeast. Nat Struct Mol Biol 2008; 15:1263-71; PMID:19011635; http://dx.doi.org/10.1038/nsmb.1514
43. Trcek T, Larson DR, Moldón A, Query CC, Singer RH. Single-molecule mRNA decay measurements reveal promoter- regulated mRNA stability in yeast. Cell 2011; 147:1484-97; PMID:22196726; http://dx.doi.org/10.1016/j.cell.2011.11.051
44. Cho RJ, Campbell MJ, Winzeler EA, Steinmetz L, Conway A, Wodicka L, Wolfsberg TG, Gabrielian AE, Landsman D, Lockhart DJ, et al. A genome-wide transcriptional analysis of the mitotic cell cycle. Mol Cell 1998; 2:65-73; PMID:9702192; http://dx.doi.org/10.1016/S1097-2765(00)80114-8
45. de Lichtenberg U, Wernersson R, Jensen TS, Nielsen HB, Fausbøll A, Schmidt P, Hansen FB, Knudsen S, Brunak S. New weakly expressed cell cycle-regulated genes in yeast. Yeast 2005; 22:1191-201; PMID:16278933; http://dx.doi.org/10.1002/yea.1302
46. Gauthier NP, Jensen LJ, Wernersson R, Brunak S, Jensen TS. Cyclebase.org: version 2.0, an updated comprehensive, multi-species repository of cell cycle experiments and derived analysis results. Nucleic Acids Res 2010; 38(Database issue):D699-702; PMID:19934261; http://dx.doi.org/10.1093/nar/gkp1044
47. Pramila T, Wu W, Miles S, Noble WS, Breeden LL. The Forkhead transcription factor Hcm1 regulates chromosome segregation genes and fills the S-phase gap in the transcriptional circuitry of the cell cycle. Genes Dev 2006; 20:2266-78; PMID:16912276; http://dx.doi.org/10.1101/gad.1450606
48. Spellman PT, Sherlock G, Zhang MQ, Iyer VR, Anders K, Eisen MB, Brown PO, Botstein D, Futcher B. Comprehensive identification of cell cycle-regulated genes of the yeast Saccharomyces cerevisiae by microarray hybridization. Mol Biol Cell 1998; 9:3273-97; PMID:9843569; http://dx.doi.org/10.1091/mbc.9.12.3273
49. de Sousa Abreu R, Penalva LO, Marcotte EM, Vogel C. Global signatures of protein and mRNA expression levels. Mol Biosyst 2009; 5:1512-26; PMID:20023718
50. Ciandrini L, Stansfield I, Romano MC. Ribosome traffic on mRNAs maps to gene ontology: genome-wide quantification of translation initiation rates and polysome size regulation. PLoS Comput Biol 2013; 9:e1002866; PMID:23382661; http://dx.doi.org/10.1371/journal.pcbi.1002866
51. Frenkel-Morgenstern M, Danon T, Christian T, Igarashi T, Cohen L, Hou YM, Jensen LJ. Genes adopt non-optimal codon usage to generate cell cycle-dependent oscillations in protein levels. Mol Syst Biol 2012; 8:572; PMID:22373820; http://dx.doi.org/10.1038/msb.2012.3
52. Tyers M, Jorgensen P. Proteolysis and the cell cycle: with this RING I do thee destroy. Curr Opin Genet Dev 2000; 10:54-64; PMID:10679394; http://dx.doi.org/10.1016/S0959-437X(99)00049-0
53. Grigull J, Mnaimneh S, Pootoolal J, Robinson MD, Hughes TR. Genome-wide analysis of mRNA stability using transcription inhibitors and microarrays reveals posttranscriptional control of ribosome biogenesis factors. Mol Cell Biol 2004; 24:5534-47; PMID:15169913; http://dx.doi.org/10.1128/MCB.24.12.5534-5547.2004
54. Miller C, Schwalb B, Maier K, Schulz D, Dümcke S, Zacher B, Mayer A, Sydow J, Marcinowski L, Dölken L, et al. Dynamic transcriptome analysis measures rates of mRNA synthesis and decay in yeast. Mol Syst Biol 2011; 7:458; PMID:21206491; http://dx.doi.org/10.1038/msb.2010.112
55. Munchel SE, Shultzaberger RK, Takizawa N, Weis K. Dynamic profiling of mRNA turnover reveals gene-specific and system-wide regulation of mRNA decay. Mol Biol Cell 2011; 22:2787-95; PMID:21680716; http://dx.doi.org/10.1091/mbc.E11-01-0028
56. Sun M, Schwalb B, Schulz D, Pirkl N, Etzold S, Larivière L, Maier KC, Seizl M, Tresch A, Cramer P. Comparative dynamic transcriptome analysis (cDTA) reveals mutual feedback between mRNA synthesis and degradation. Genome Res 2012; 22:1350-9; PMID:22466169; http://dx.doi.org/10.1101/gr.130161.111
57. Winsor B, Schiebel E. Review: an overview of the Saccharomyces cerevisiae microtubule and microfilament cytoskeleton. Yeast 1997; 13:399-434; PMID:9153752; http://dx.doi.org/10.1002/(SICI)1097-0061(199704)13:5<399::AID-YEA126>3.0.CO;2-9
58. Hocine S, Raymond P, Zenklusen D, Chao JA, Singer RH. Single-molecule analysis of gene expression using two-color RNA labeling in live yeast. Nat Methods 2013; 10:119-21; PMID:23263691; http://dx.doi.org/10.1038/nmeth.2305
59. Huh WK, Falvo JV, Gerke LC, Carroll AS, Howson RW, Weissman JS, O'Shea EK. Global analysis of protein localization in budding yeast. Nature 2003; 425:686-91; PMID:14562095; http://dx.doi.org/10.1038/nature02026
60. Allan C, Burel JM, Moore J, Blackburn C, Linkert M, Loynton S, Macdonald D, Moore WJ, Neves C, Patterson A, et al. OMERO: flexible, model-driven data management for experimental biology. Nat Methods 2012; 9:245-53; PMID:22373911; http://dx.doi.org/10.1038/nmeth.1896
61. Haase SB, Reed SI. Improved flow cytometric analysis of the budding yeast cell cycle. Cell Cycle 2002; 1:132-6; PMID:12429922; http://dx.doi.org/10.4161/cc.1.2.114
62. Edelstein A, Amodaj N, Hoover K, Vale R, Stuurman N. Computer control of microscopes using μManager. Curr Protoc Mol Biol 2010; Chapter 14:Unit14 20.
63. Cohen J. Statistical power analysis for the behavioral sciences. Hillsdale, N.J.: L. Erlbaum Associates, 1988.
64. Di Talia S, Wang H, Skotheim JM, Rosebrock AP, Futcher B, Cross FR. Daughter-specific transcription factors regulate cell size control in budding yeast. PLoS Biol 2009; 7:e1000221; PMID:19841732; http://dx.doi.org/10.1371/journal.pbio.1000221